energies

MDPI

Article

Primary Voltage and Frequency Regulation in Inverter Based Islanded Microgrids through a Model Predictive Control Approach

Daniele Mestriner [1,*], Alessandro Rosini [1], Iris Xhani [2], Andrea Bonfiglio [1] and Renato Procopio [1]

[1] Naval, Electrical, Electronics and Telecommunication Engineering and Naval Architecture Department (DITEN), University of Genoa, Via All'Opera Pia 11a, 16145 Genoa, Italy; alessandro.rosini@edu.unige.it (A.R.); a.bonfiglio@unige.it (A.B.); renato.procopio@unige.it (R.P.)
[2] RINA Consulting S.p.A., Via A. Cecchi, 6-16129 Genoa, Italy; xhani.iris@gmail.com
* Correspondence: daniele.mestriner@edu.unige.it

Abstract: A frequency and voltage control strategy based on a decentralized and communication-less approach is proposed in this work and applied to Photovoltaic-Storage-Microturbine islanded Microgrids (MGs). The approach is based on the Model Predictive Control (MPC) technique. Thanks to the use of local measurements, each source can nullify the steady-state voltage and frequency errors by means of a dedicated MPC controller. Consequently, the proposed approach unifies the advantages of classic droop and master/slave controllers due to the absence of communication links among devices and due to the absence of a secondary centralized control loop.

Keywords: microgrids; model predictive control; frequency regulation

Citation: Mestriner, D.; Rosini, A.; Xhani, I.; Bonfiglio, A.; Procopio, R. Primary Voltage and Frequency Regulation in Inverter Based Islanded Microgrids through a Model Predictive Control Approach. *Energies* **2021**, *15*, 5077. https://doi.org/10.3390/en15145077

Academic Editor: Abu-Siada Ahmed

Received: 1 April 2022
Accepted: 11 July 2022
Published: 12 July 2022

1. Introduction

The reduction of greenhouse gas emission to at least 55% compared to 1990 can be achieved also thanks to a deep integration of Renewable Energies Sources (RES) in the energy sector [1].

In this framework, the transition toward this scenario should be strongly connected to an improvement of the system flexibility [2,3]. The flexibilization of power generation, transmission, distribution and consumption is nowadays an important research topic strongly supported by the European Union, as shown in different international projects [4].

Microgrids (MGs) represent an optimal way to integrate RES into the electrical system, since an MG is defined as an integrated energy system consisting of Distributed Energy Resources (DER) and multiple electrical loads operating as a single grid either in parallel to or islanded from the existing distribution power grid [5].

While the MG operation is quite straightforward during grid-connected operation, if an islanded mode is required, the control logics and the management system should be carefully checked. During islanded operation, due to the lack of the primary voltage source (i.e., the main grid), the primary regulation of the MG is a difficult task that is normally achieved according to two ways:

- Communication-based control techniques;
- Communication-less control techniques.

Communication-based techniques include the master–slave control [6,7] and the distributed control [8] among others; they require a communication link between the different energy sources and loads of the MG, which can be expensive in rural areas or in case of long distances among the energy sources.

On the other hand, when we deal with communication-less techniques, we usually refer to the well-known droop control [9,10]. This approach can provide good results in terms

of energy sharing among the sources, but it presents two main drawbacks: (i) frequency and voltage are not restored to their rated values, resulting in the need of secondary regulation and (ii) no multiple objectives can be pursued.

Model Predictive Control (MPC) [11] has been applied to MGs in the last few years [12–14] focusing on economical aspects (tertiary control) or in specific applications [12]. Recently, in [15], an innovative control method based on the MPC has been proposed and applied to an MG that consists of only photovoltaic (PV) and storage (ST) units. According to [15], the proposed control system avoids the disadvantages of communication-based and communication-less control systems, achieving the goals of primary regulation and secondary regulation without communication and guaranteeing an automatic and seamless transition among the different MG operating assets without communication. In addition to [15], other works have focused their efforts on trying to find a suitable solution through the application of the MPC technique during the MG primary regulation. In [16,17], the MPC controller has been used instead of the PID regulators in order to achieve better dynamics, but the controller is inserted in a droop control logic, which still has to face the problems of frequency and voltage deviations at steady state.

This work proposes the extension of the decentralized control system defined in [15] to an MG formed by a PV unit, an ST and a microturbine (MT) connected to the AC MG distribution system via a power elecrtonic converter, as shown in Figure 1. The control system described in the paper guarantees the restoration of voltage and frequency inside their limits when a contingency occurs without the need of a communication link among the sources. Moreover, the proposed control system is able to avoid the steady-state frequency deviation, which can be usually found in the droop-control technique. Finally, the specific nature of the three energy sources is accounted in the three controllers in order to prevent the control system from producing unfeasibile working points in the MG. The paper is organized as follows: Section 2 describes the general structure of the system, Section 3 recalls the main principles of the MPC control system and shows the details of the MT MPC controller, and Section 4 analyzes the different operating scenarios. Finally, Section 5 is dedicated to the simulations and conclusions.

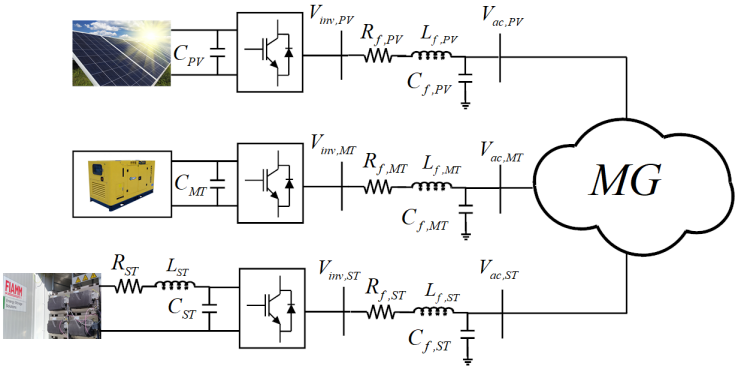

Figure 1. General layout.

2. MPC Controllers: Theory and Design

This section briefly recalls the main concepts of the MPC theory and proposes the design of the MPC controllers of each source.

2.1. MPC Theory

Let consider the following linear time-invariant discrete system:

$$x_{k+1} = A_k x_k + B_k u_k + f_k \tag{1}$$

where x_k and u_k are the states and the input at time kT_s, in which T_s is the sampling time. Another quantity y_k defined as a linear combination of states and inputs that can be obtained as follows:

$$y_k = a_k x_k + b_k u_k + c_k \tag{2}$$

The MPC controller acts to regulate the states of the system to a reference value x_{ref} and the inputs to a reference value u_{ref} by solving the constrained Quadratic-Programming (QP) problem. Please note that N is the prediction horizon and $Q = Q^T$, $R = R^T$, $S = S^T$, are symmetric semi-definite weighting matrices.

$$\begin{aligned} \min_U \quad \sum_{i=0}^{N-1} (x - x_{ref})^T_{k+i|k} Q (x - x_{ref})_{k+i|k} + (u - u_{ref})^T_{k+i} R (u - u_{ref})_{k+i} \\ + (y - y_{ref})^T_{k+i} S (y - y_{ref})_{k+i} \end{aligned} \tag{3}$$

Defining the error vectors as:

$$\begin{aligned} X &= (x - x_{ref}) \\ U &= (u - u_{ref}) \\ Y &= (y - y_{ref}) \end{aligned} \tag{4}$$

Equation (3) becomes

$$\min_U \quad \sum_{i=0}^{N-1} \left\{ X^T_{k+i|k} Q X_{k+i|k} + U^T_{k+i} R U_{k+i} + Y^T_{k+i} S Y_{k+i} \right\} \tag{5}$$

where

$$X_{k+i+1|k} = A_{k+i} X_{k+i|k} + B_{k+i} U_{k+i} + f_{k+i} \tag{6}$$

represents the prediction of the state evaluated at time kT_s, where T_s is the sampling time. Generally, some constraints can be set to the inputs, state variables and mixed state-input variables. They can be outlined in the following form:

$$\begin{aligned} H_u U_{k+i} &\leq K_u, \; i = 0, \ldots, N-1 \\ H_x X_{k+i} &\leq K_x, \; i = 0, \ldots, N-1 \\ H_y Y_{k+i} &\leq K_y, \; i = 0, \ldots, N-1 \end{aligned} \tag{7}$$

In addition to this, also, mixed state input constraints can also be imposed as follows:

$$F_x X_{k+1} + E_x U_{k+1} \leq G_x \tag{8}$$

where $H_u, K_u, H_x, K_x, H_y, K_y, F_x, E_x$, and G_x are matrices that define the constraints for the controlled system. Substituting (2) and (4) into (5), one obtains that

$$\begin{aligned} \min_U \quad \sum_{i=0}^{N-1} X^T_{k+i|k} Q X_{k+i|k} + U^T_{k+i} R U_{k+i} \\ + (a_{k+i} X_{k+i|k} + b_{k+i} U_{k+i} + c_{k+i})^T S (a_{k+i} X_{k+i|k} + b_{k+i} U_{k+i} + c_{k+i}) \end{aligned} \tag{9}$$

Performing the calculations, it is possible to obtain:

$$\begin{aligned}
&\min_{U} \quad \sum_{i=0}^{N-1} [X_{k+i|k}^T Q X_{k+i|k} + U_{k+i}^T R U_{k+i} + \\
&(a_{k+i} X_{k+i|k} + b_{k+i} U_{k+i} + c_{k+i})^T S (a_{k+i} X_{k+i|k} + b_{k+i} U_{k+i} + c_{k+i})] \\
&= X_{k+N}^T Q X_{k+N} + \sum_{i=0}^{N-1} [X_{k+i|k}^T Q X_{k+i|k} + U_{k+i}^T R U_{k+i} + \\
&X_{k+i|k}^T a_{k+i}^T S a_{k+i} X_{k+i|k} + X_{k+i|k}^T a_{k+i}^T S b_{k+i} U_{k+i} + X_{k+i|k}^T a_{k+i}^T S c_{k+i} + \\
&U_{k+i}^T b_{k+i}^T S a_{k+i} X_{k+i|k} + U_{k+i}^T b_{k+i}^T S b_{k+i} U_{k+i} + U_{k+i}^T b_{k+i}^T S c_{k+i} + \\
&c_{k+i}^T S a_{k+i} X_{k+i|k} + c_{k+i}^T S b_{k+i} U_{k+i} + c_{k+i}^T S c_{k+i}]
\end{aligned} \tag{10}$$

Neglecting the term ${c_{k+i}}^T S c_{k+i}$ (it is a constant and it does not affect the calculation of the minimum), it is possible to obtain the following equation:

$$\begin{aligned}
&\min_{U} \quad \sum_{i=0}^{N-1} [X_{k+i|k}^T (Q + a_{k+i}^T S a_{k+i}) X_{k+i|k} + U_{k+i}^T (R + b_{k+i}^T S b_{k+i}) U_{k+i} \\
&+ a_{k+i}^T {X^T}_{k+i|k} S b_{k+i} U_{k+i} + b_{k+i}^T {U^T}_{k+i} S a_{k+i} X_{k+i|k} \\
&+ 2 c_{k+i}^T S a_{k+i} X_{k+i|k} + 2 c_{k+i}^T S b_{k+i} U_{k+i}
\end{aligned} \tag{11}$$

In order to compact (11), it is possible to introduce the following matrix:

$$\tilde{X} = \begin{bmatrix} U \\ X \end{bmatrix} \tag{12}$$

and consequently

$$\min_{U} \quad \sum_{i=0}^{N-1} \left[\tilde{X}_{k+i}^T F_{k+i} \tilde{X}_{k+i} + f_{k+i}^T \tilde{X}_{k+i} \right] \tag{13}$$

where $F_k = \begin{bmatrix} R + b_k^T S b_k & b_k^T S a_k \\ a_k^T S b_k & Q + a_k^T S a_k \end{bmatrix}$ and $f_k = \begin{bmatrix} c_k^T S b_k \\ c_k^T S a_k \end{bmatrix}$.

The MPC controller generates the control action using this strategy: the optimization problem is solved at each step, as shown in Equation (13). Secondly, the controller evaluates the prediction of the state variables and computes the input to be provided within the control horizon. Finally, the first solution of the optimal input U_k is applied to the controlled system. Please note that if the model is not linear, a linearization procedure is required in order to obtain the system described in (1).

2.2. Design of the MPC Controllers

In this subsection, the design of the controllers of the power converters of the three main source units (ST, PV, MT) that can be found in many islanded MGs is presented. Each converter is equipped with an MPC local controller, where an optimization problem in the form of (5) has to be set up, where the objective function allows regulating states, inputs and their linear combination to some desired values.

The design of each controller is made providing some assumptions to the so-called auxiliary model (i.e., the model adopted to design the controllers, which is in the form of (1)). They are:

- The MG AC section is supposed to be at steady state [18];
- Power converters are supposed to work in their linear range;
- Power converters efficiency is assumed to be unitary;
- Higher order harmonics are neglected;

- Shunt section and resistive component for the harmonic filter are neglected.

Please note that these assumptions are only made for the design of the controllers, while in the simulations section, the MG components and the infrastructure are represented with a much higher level of detail, thus allowing to test the robustness of the proposed control structure. Note also that the model relying on the above assumptions has been validated with field measurements in [18].

In the following three subsections, details of the MPC controllers are presented. Such controllers change the quantities to be regulated (i.e., the MPC objective function) according to the different functionalities that the source has to cover. The functionalities correspond to the different operation mode each inverter has to work and may be divided into two main categories: grid-forming inverters (that control voltage and frequency) and grid-feeding ivnerters (that control active and reactive power). Details on the operation modes and on the transition among them are provided in Section 4.

2.2.1. MT Controller Design

The MT is modeled as a driven current generator interfaced with a DC/AC converter. Let us consider the MT unit depicted in Figure 1: the line-to-ground RMS voltage at the inverter output is

$$\hat{V}_{inv,MT}(t) = \frac{m_{a,MT}(t)V_{dc,MT}(t)}{2\sqrt{2}} e^{j\theta_{MT}(t)} \tag{14}$$

where $m_{a,MT}$ is the inverter modulation index, $V_{dc,MT}$ is the DC-link voltage and θ_{MT} is given by

$$\theta_{MT}(t) = \int_0^t \omega_{MT}(\tau)d\tau + \theta_{MT0} \tag{15}$$

where ω_{MT} is the angular frequency of the inverter modulation signals and θ_{MT0} is the MT voltage initial phase.

The MT voltage at the harmonic-filter output can be written as:

$$\hat{V}_{ac,MT}(t) = V_{ac,MT}(t)e^{j\theta_{f,MT(t)}} \tag{16}$$

where $V_{ac,MT}$ is the phase voltage at the harmonic-filter output and $\theta_{f,MT}(t)$ is given by

$$\theta_{f,MT}(t) = \int_0^t \omega_{f,MT}(\tau)d\tau + \varphi_{f,MT}(t) \tag{17}$$

$\omega_{f,MT}$ being the AC-bus angular frequency measured via PLL and $\varphi_{f,MT}(t)$ being the phase angle of $V_{ac,MT}$.

For the sake of readability, from now on, the explicit time dependence will be omitted.

Neglecting $R_{f,MT}$, the active power flow injected by the MT unit into the MG is given by:

$$P_{ac,MT} = 3\frac{m_{a,MT}V_{dc,MT}V_{ac,MT}}{2\sqrt{2}x_f} \sin\left(\theta_{MT} - \theta_{f,MT}\right) \tag{18}$$

where x_f is the inductive reactance of the harmonic filter at the rated frequency. Substituting (15) and (17) into (18), one can easily obtain:

$$P_{ac,MT} = \frac{3m_{a,MT}V_{dc,MT}V_{ac,MT}}{2\sqrt{2}x_f} \sin\left(\theta_{MT0} - \varphi_{f,MT} + \int_0^t (\omega_{MT} - \omega_{f,MT})d\tau\right) \tag{19}$$

Let us now define:

$$\sigma_{MT} = \theta_{MT0} - \varphi_{f,MT} \tag{20}$$

and

$$\delta_{MT} = \int_0^t \Big(\omega_{MT}(\tau) - \omega_{f,MT}(\tau)\Big) d\tau \tag{21}$$

Inserting (20) and (21) into (19), one obtains:

$$P_{ac,MT} = 3\frac{m_{a,MT} V_{dc,MT} V_{ac,MT}}{2\sqrt{2} x_f} \sin(\sigma_{MT} + \delta_{MT}) \tag{22}$$

which enters the DC-link voltage dynamics:

$$P_{dc,MT} - P_{ac,MT} = V_{dc,MT} C_{MT} \frac{dV_{dc,MT}}{dt} \tag{23}$$

where C_{MT} is the DC-link capacitor and $P_{dc,MT}$ is the power coming from the MT unit. It is well known that in an MT, there is a delay between the request of a certain amount of power and the delivered one. Thus, it is necessary to take into account the dynamics of the MT, which accounts at least for the time needed to provide the required power ($P^*_{dc,MT}$).

According to Figure 2 and referring to [19], the following relationship can be written, where X is an auxiliary state:

$$\begin{cases} T_2 \frac{dP_{DC,MT}}{dt} + P_{DC,MT} = X \\ T_1 \frac{dX}{dt} + X = P^*_{DC,MT} \end{cases} \tag{24}$$

That corresponds to the scheme depicted in Figure 2.

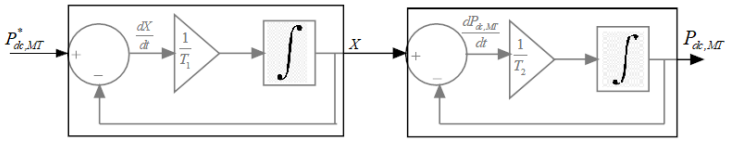

Figure 2. MT dynamic model.

From (21) and (24), it follows that:

$$\begin{cases} \frac{dV_{dc,MT}}{dt} = \frac{1}{C_{MT}} \left[\frac{P_{dc,MT}}{V_{dc,MT}} - \frac{3 m_{a,MT} V_{ac,MT}}{2\sqrt{2} x_f} \sin(\sigma_{MT} + \delta_{MT}) \right] \\ \frac{d\delta_{MT}}{dt} = \omega_{MT} - \omega_{f,MT} \\ \frac{dP_{dc,MT}}{dt} = \frac{X - P_{dc,MT}}{T_2} \\ \frac{dX}{dt} = \frac{P^*_{dc,MT} - X}{T_1} \end{cases} \tag{25}$$

The system presented in (25) represents the physical dynamics of the MT. Moreover, as the modulation index has to remain constant at steady state regardless of the value it assumes in the range [0, 1], one can introduce its derivative $J_{m,MT}$ as a new variable and then set its reference value to zero.

The new system becomes:

$$\begin{cases} \frac{dV_{dc,MT}}{dt} = \frac{1}{C_{MT}} \left[\frac{P_{dc,MT}}{V_{dc,MT}} - \frac{3 m_{a,MT} V_{ac,MT}}{2\sqrt{2} x_f} \sin(\sigma_{MT} + \delta_{MT}) \right] \\ \frac{d\delta_{MT}}{dt} = \omega_{MT} - \omega_{f,MT} \\ \frac{dP_{dc,MT}}{dt} = \frac{X - P_{dc,MT}}{T_2} \\ \frac{dX}{dt} = \frac{P^*_{dc,MT} - X}{T_1} \\ \frac{dm_{a,MT}}{dt} = J_{m,MT} \end{cases} \tag{26}$$

The new system inputs are $P^*_{dc,MT}$, ω_{MT} and $J_{m,MT}$, while $V_{dc,MT}$, δ_{MT}, $P_{dc,MT}$, X and $m_{a,MT}$ are the states.

System (26) is a non-linear continuous-time system in the form:

$$\dot{x}_{MT} = f(x_{MT}, u_{MT}, g_{MT}) \tag{27}$$

where $u_{MT} = \left[\omega_{MT},\ P^*_{dc,MT}\ J_{MT}\right]^T$ is the input vector, $x_{MT} = \left[V_{dc,MT}\ \ \delta_{MT}\ P_{dc,MT}\ \ X\ m_{a,MT}\ \right]^T$ is the state vector and $g_{MT} = \left[V_{ac,MT}\ \sigma_{MT}\ \omega_{f,MT}\right]^T$ is a vector that collects measurements and estimated variables. In particular, $V_{ac,MT}$ and $\omega_{f,MT}$ can be easily measured, while σ_{MT} can be estimated measuring the MT AC side active power and inverting (22) as follows:

$$\sigma_{MT} = \sin^{-1}\left(\frac{2\sqrt{2}P_{ac,MT}x_f}{3m_{a,MT}V_{dc,MT}V_{ac,MT}}\right) - \int_0^t \left(\omega_{MT}(\tau) - \omega_{f,MT}(\tau)\right)d\tau \tag{28}$$

A detailed representation of the MT MPC controller can be found in Figure 3.

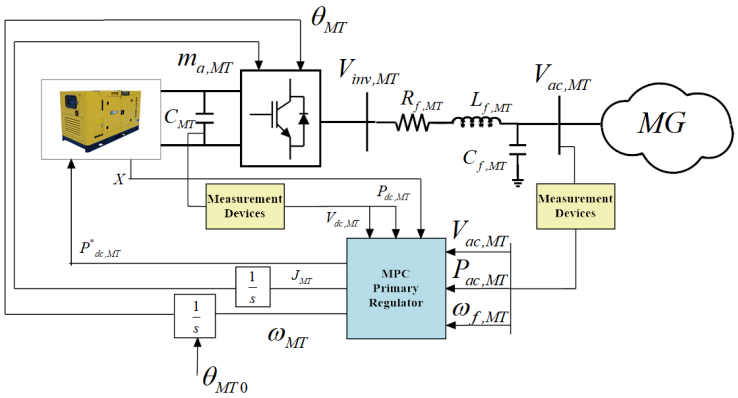

Figure 3. MT Control scheme.

Since the time evolution of measurements is unknown during the prediction, they are supposed to remain constant, which corresponds to set:

$$g_{MT,k+1} = g_{MT,k} \tag{29}$$

The mathematical model for the prediction in MPC controllers can be obtained linearizing and discretizing (26). The linearization process is done for each time step k and leads to an equation such as:

$$\frac{dx_{MT,k}}{dt} = A_{MT,k}x_{MT,k} + B_{MT,k}u_{MT,k} + D_{MT,k} \tag{30}$$

where $A_{MT,k}$, $B_{MT,k}$, $C_{MT,k}$, and $D_{MT,k}$ are matrices obtained by partial derivation operations with respect to states, inputs and measurements, respectively. Once obtained, it is possible to discretize them through the following logic:

$$\frac{dx_{MT}}{dt} = \frac{x_{MT,k+1} - x_{MT,k}}{T_S} \tag{31}$$

Then, substituting (30) into (31), one obtains:

$$x_{MT,k+1} = (I + T_S A_{MT,k})x_{MT,k} + T_S B_{MT,k}u_{MT,k} + T_S C_{MT,k}g_{MT,k} + T_S D_{MT,k} \tag{32}$$

where $x_{MT,k}$, $u_{MT,k}$ and $g_{MT,k}$ indicate state, inputs and measurements, respectively, at time kT_s.

Since the MPC equation must be in the form (6), it is necessary to combine states and measurements in a single matrix, obtaining:

$$\tilde{x}_{MT,k} = \begin{bmatrix} x_{MT,k} \\ g_{MT,k} \end{bmatrix} \tag{33}$$

$$\tilde{x}_{MT,k+1} = \begin{bmatrix} x_{MT,k+1} \\ g_{MT,k+1} \end{bmatrix} = \begin{bmatrix} I + T_S A_{MT,k} & T_S C_{MT,k} \\ 0 & I \end{bmatrix} \begin{bmatrix} x_{MT,k} \\ g_{MT,k} \end{bmatrix} + \begin{bmatrix} T_S B_{MT,k} \\ 0 \end{bmatrix} u_{MT,k} + \begin{bmatrix} T_S D_{MT,k} \\ 0 \end{bmatrix} \tag{34}$$

Finally, renaming the matrices of (34), it is possible to obtain:

$$\tilde{x}_{MT,k+1} = A_{d,MT,k}\tilde{x}_{MT,k} + B_{d,MT,k}u_{MT,k} + f_{d,MT,k} \tag{35}$$

The MT MPC controller can regulate states, inputs and functions of states and inputs to a desired value. The latter case is typically represented by the reactive power, which can be expressed as a function of states and inputs as follows:

$$Q_{MT,k} = 3\left[\frac{m_{a,MT,k}^2 V_{dc,MT,k}^2}{8x_f} - \frac{m_{a,MT,k} V_{dc,MT,k} V_{ac,MT,k}}{2\sqrt{2}x_f}\cos(\sigma_{MT,k} + \delta_{MT,k})\right] \tag{36}$$

Unlike the other quantities, the reactive power is neither a state nor an input. On the contrary, (36) is a non-linear combination of states and inputs, so one can linearize it in order to have a linear relation in the form of (2) and then treat it as an objective in order to reach its reference value $Q_{MT,ref}$.

The linearization process leads to an equation such as

$$Q_{MT,k} = a_{MT,k}\tilde{x}_{MT,k} + b_{MT,k}u_{MT,k} + c_{MT,k} \tag{37}$$

Please note that (37) has the same structure as Equation (2). $a_{MT,k}$, $b_{MT,k}$, and $c_{MT,k}$ are matrices obtained by partial derivation operations for each time step k with respect to the states and inputs, respectively.

The MT MPC control system objectives vary according to the operation mode. Its behavior can be divided in two different modes.

- Slack node: the controller regulates $\omega_{f,MT}$ and $J_{m,MT}$ (grid-forming inveters);
- PQ node: the controller regulates $P_{dc,MT}$ and $Q_{MT,k}$ (grid-feeding inverter).

The constraints of this controller are:

- To limit the DC active power into a boundary level such that: $0 \leq P_{DC,MT} \leq P_{DC,MT\,\max}$;
- The MT unit frequency does not have to exceed the minimum limit $f_{\min}$ and the maximum limit $f_{\max}$ as well, so: $2\pi f_{\min} \leq \omega_{MT,k} \leq 2\pi f_{\max}$;
- Even during transients, the inverter capability curve is never exceeded: $\sqrt{P_{ac,MT}^2 + Q_{MT}^2} \leq A_{\max,MT}$, where $A_{\max,MT}$ is the rated inverter capability;
- the MT AC voltage does not have to exceed the minimum limit $V_{AC,min,MT}$ and the maximum limit $V_{AC,max,MT}$.

It is important to focus more attention on the last constraint related to the AC voltage. In order to satisfy it, it should be noted that the AC voltage can be expressed as follows:

$$V_{ac,MT} = \frac{m_{a,MT} V_{dc,MT}}{2\sqrt{2}} - \Delta v \tag{38}$$

where Δv is the voltage drop on the harmonic filter, which can be expressed with the typical voltage drop expression:

$$\Delta v = \frac{1}{3V_{ac,MT}}(R_{f,MT}P_{ac,MT} + X_{f,MT}Q_{MT}) \tag{39}$$

where R_f is the longitudinal resistance of the harmonic filter. Consequently, the problem can be expressed as a linear constraint involving the states $V_{dc,MT}$ and $m_{a,MT}$ at each time step k.

$$V_{AC,min,MT} + V^*_{ac,MT} + \Delta v \leq \frac{m_{a,MT,k} V_{dc,MT,k}}{2\sqrt{2}} \leq \Delta v + V^*_{ac,MT} + V_{AC,max,MT} \quad (40)$$

Since the MPC problem has been set using linear equations, the linearization of (40) is mandatory.

2.2.2. PV Controller Design

The details of the PV control design can be found in [15]. For the sake of completeness, here, the following variables are recalled and used:

- $V_{DC,PV}$: PV DC-link voltage
- $\omega_{f,PV}$: PV inverter modulation frequency;
- $m_{a,PV}$: PV inverter modulation amplitude;
- J_{PV}: PV inverter modulation amplitude time derivative;
- Q_{PV}: PV reactive power ;
- $V_{AC,PV}$: PV AC phase voltage;
- α: solar irradiance;
- T: cell temperature.

The PV MPC control system objectives are always related to the behavior of the PV system as a PQ node, i.e., to the control of the active and reactive power injections by setting $V_{DC,PV}$ to its maximum power point (MPP) and by setting Q_{PV} to a reference value according to the same procedure proposed for the MT in (36), (37) and also described in [15].

2.2.3. ST Controller Design

The details of the ST control design can be found in [15]. For the sake of completeness, here, the following variables are recalled and used:

- $V_{DC,ST}$: Storage DC-link voltage;
- $\omega_{f,ST}$: Storage inverter modulation frequency;
- $m_{a,ST}$: Storage inverter modulation amplitude;
- J_{ST}: Storage inverter modulation amplitude time derivative;
- Q_{ST}: Storage reactive power;
- $I_{DC,ST}$: Storage DC-link current;
- $V_{AC,ST}$: Storage AC phase voltage;
- SOC: Storage state of charge.

The ST MPC control system objectives vary according to the operation mode. Its behavior can be divided in two different modes:

- Slack bus: the controller regulates $\omega_{f,ST}$ and $J_{m,ST}$;
- PQ bus: the controller regulates $V_{DC,ST}$ (and consequently its power injection) and Q_{ST}.

As a conclusion, each source (MT, ST and PV) regulates different variables according to the different mode (slack or PQ bus). The summary is presented in Table 1.

Table 1. Control objectives.

Source	Slack Bus	PQ Bus
ST	$\omega_{f,ST}$ and $J_{m,ST}$	$V_{DC,ST}$ and Q_{ST}
PV	-	$V_{DC,PV}$ and Q_{PV}
MT	$\omega_{f,MT}$ and $J_{m,MT}$	$P_{DC,MT}$ and Q_{MT}

3. Operation Modes

This section describes the operation modes of the MG and the corresponding logics that each controller has to implement.

The PV, ST and MT active and reactive power exchanges are initially set by an Energy Management System (EMS), which defines each working point.

Starting from it, two possible contingencies can be observed:

1. A negative unbalance of active power, i.e., the power production is lower than the power consumption.
2. A positive unbalance of active power, i.e., the power production is higher than the power consumption.

The power unbalance is always detected by each MPC controller as a variation in the DC-link voltages ($V_{DC,MT}$, $V_{DC,ST}$, $V_{DC,PV}$). A positive unbalance causes an enhancement of the DC-link voltage, while a negative unbalance causes a decrease.

A summarizing flowchart of the possible operation modes is proposed in Figure 4.

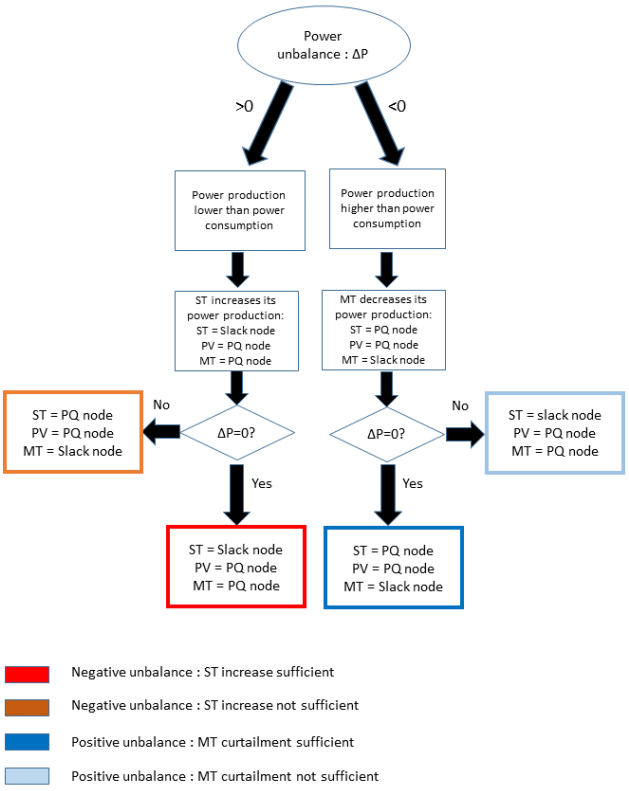

Figure 4. Flowchart of the operation modes.

3.1. Negative Unbalance

When a negative unbalance occurs, the power production is lower than the power consumption. Consequently, in order to restore the balance, a energy source should increase its production. The first energy source that has to intervene is the ST, since the PV is already delivering its MPP, and an increase in the MT power would be associated to the fuel cost, which is economically inconvenient. This leads to two different options:

1. The increase provided by the ST is sufficient to restore the balance.
2. The increase provided by the ST is not sufficient to restore the balance, as it reaches its maximum power deliverable.

3.1.1. ST Increase Sufficient

When the ST increase is sufficient, the PV and the MT behave as PQ nodes and maintain the active and reactive power previously defined by the EMS. The ST is a slack node, controlling the voltage and the frequency of the MG.

3.1.2. ST Increase not Sufficient

Initially, the ST behaves as a slack node, increasing its power production, until it reaches its maximum power deliverable or its minimum state of charge. From now onward, the ST and the PV unit behave as PQ nodes, while the MT behaves a slack node in order to restore the balance. The ST unit operates as a PQ node by setting the DC-link voltage to the value corresponding to the ST maximum power. The transition of the MT from PQ mode to slack mode is guaranteed by a second decrease of the DC link voltage, which is the variable responsible for the mode operation change.

3.2. Positive Unbalance

When a positive unbalance occurs, the power production is higher than the power consumption. Consequently, in order to restore the balance, a energy source should be curtailed.

The first energy source that has to act is the MT, since it is more economically convenient than reducing the ST or PV production.

This leads to two different options:

1. The curtailment provided by the MT is sufficient to restore the balance.
2. The curtailment provided by the MT is not sufficient to restore the balance.

3.2.1. MT Curtailment Sufficient

When the MT curtailment is enough, the ST and PV unit act as PQ nodes; i.e., they maintain the active and reactive power previously defined by the EMS.

The MT behaves as a slack node, controlling the voltage and the frequency of the MG.

3.2.2. MT Curtailment not Sufficient

Initially, the MT behaves as a slack node, reducing its power production until it becomes zero. From now onward, the MT and the PV unit behave as PQ nodes, while the ST acts as a slack node in order to restore the balance.

The transition of the ST from PQ mode to slack mode is guaranteed by a second enhancement of the DC link voltage, which is the variable responsible for the mode operation change.

4. Simulations and Results

The proposed control system has been applied to the MG described in [18] and depicted in Figure 5.

The peak power of the PV unit is 16 kW, while the corresponding inverter rating is 17 kVA. For the ST, the Nominal Current Capacity (NCC) is 228 Ah, while the power limits are 25 kW (when the ST is charging) and 60 kW (when the ST is discharging) and the inverter rating is 62 kVA. The power limit of the MT is, on the other hand, 30 kW, and the inverter rating is 35 kVA.

The load is simulated as constant impendance and is directly connected to the main bus of the MG. The simulation environment is Simulink/Simscape®, where inverters are modeled as two-level IGBT converters and the modulation is achieved by means of the PWM techique with a 10 kHz carrier signal. On the other hand, the PV unit is modeled as suggested in [18], and the ST model is provided in [20]. Finally, the MT is modeled as proposed in Section 3, considering T_1 = 0.4 s and T_2 = 0.1 s.

Cables are modeled by means of R-L series, while transformers are represented with the only leakage inductance. Numerical values of the sources and grid parameters appear in Tables 2 and 3, respectively.

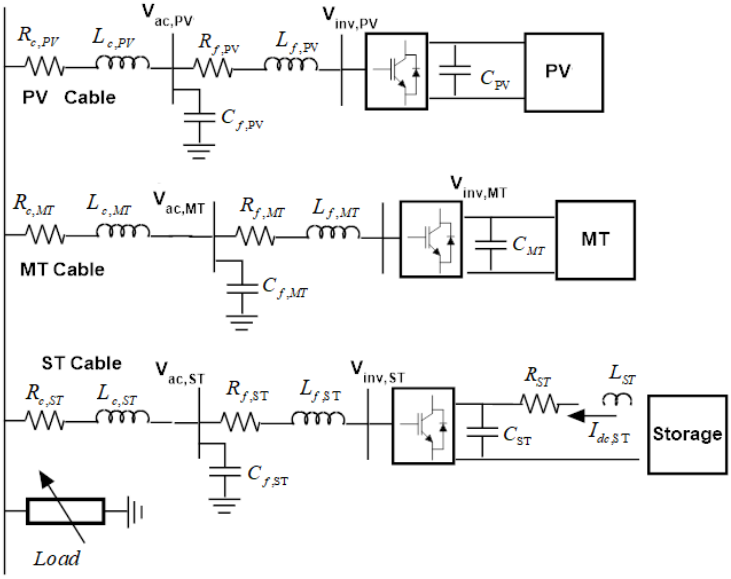

Figure 5. One-line diagram of test case MG.

Table 2. Source parameters.

PV		ST		MT	
C_{PV}	3.3 mF	C_{ST}	3 mF	C_{MT}	3 mF
$R_{f,PV}$	3.14 mΩ	R_{ST}	1.12 mΩ	$R_{f,MT}$	3.14 mΩ
$L_{f,PV}$	1 mH	L_{ST}	1 mH	$L_{f,MT}$	1 mH
$C_{f,PV}$	10 µF	$R_{f,ST}$	3.14 mΩ	$C_{f,MT}$	10 µF
		$L_{f,ST}$	1 mH		
		$C_{f,ST}$	10 µF		

Table 3. Grid parameters.

PV		ST		MT	
$R_{c,PV}$	0.15 Ω	$R_{c,ST}$	0.04 Ω	$R_{c,MT}$	0.02 Ω
$L_{c,PV}$	3.27 mH	$L_{c,ST}$	0.03 mH	$L_{c,MT}$	0.01 mH

In order to completely define the simulation's details, the parameters of each MPC controller are provided. As previously specified, two sets of control parameters should be defined for the ST and the MT, while the PV unit requires one set of control parameters. The MT PQ mode and Slack mode are defined in Tables 4 and 5, while the ST PQ and Slack modes are defined in Tables 6 and 7. Finally, the PV regulator parameters (PQ mode) are defined in Table 8.

Table 4. MT Controller parameters. Slack mode.

MT Objectives		MT Constraints	
$V_{DC,MT}$	-	P_{max}	30 kW
$P^{*}_{DC,MT}$	-	f_{min}	49.5 Hz
$\omega_{f,MT}$	314 rad/s	f_{max}	50.5 Hz
$J_{m,MT}$	0	$A_{max,MT}$	35 kVA
$Q_{MT,ref}$	-	$V_{AC,min,MT}$	218.5 V
		$V_{AC,max,MT}$	241.5 V

Table 5. MT Controller parameters. PQ mode.

MT Objectives		MT Constraints	
$V_{DC,MT}$	800 V	P_{max}	30 kW
$P^*_{DC,MT}$	$P_{DC,MT,EMS}$	f_{min}	49.5 Hz
$\omega_{f,MT}$	-	f_{max}	50.5 Hz
$J_{m,MT}$	0	$A_{max,MT}$	35 kVA
$Q_{MT,ref}$	0 VAr	$V_{AC,min,MT}$	218.5 V
		$V_{AC,max,MT}$	241.5 V

Table 6. ST Controller parameters. Slack mode.

ST Objectives		ST Constraints	
$\omega_{f,ST}$	314 rad/s	SOC_{lim}	99.5%
$J_{m,ST}$	0	f_{min}	49.5 Hz
$V_{DC,ST}$	-	f_{max}	50.5 Hz
		$A_{max,ST}$	62 kVA
		$V_{ac,ST,max}$	233 V
		$V_{ac,ST,min}$	227 V
		$P_{dc,ST,max}$	60 kW
		$P_{dc,ST,min}$	−20 kW

Table 7. ST Controller parameters. PQ mode.

ST Objectives		ST Constraints	
$\omega_{f,ST}$	-	SOC_{lim}	99.5%
$J_{m,ST}$	0	f_{min}	49.5 Hz
$V_{DC,ST}$	corresponding to $P_{DC,ST,max}$	f_{max}	50.5 Hz
		$A_{max,ST}$	62 kVA
		$V_{ac,ST,max}$	233 V
		$V_{ac,ST,min}$	227 V
		$P_{dc,ST,max}$	60 kW
		$P_{dc,ST,min}$	−20 kW

Table 8. PV Controller parameters. PQ mode.

PV Objectives		PV Constraints	
$V_{DC,PV}$	$V_{DC,PV,MPPT}$	f_{min}	49.5 Hz
$\omega_{f,PV}$	-	f_{max}	50.5 Hz
$J_{m,PV}$	0	$A_{max,PV}$	24 kVA
$Q_{PV,ref}$	0 VAr	$V_{AC,min,PV}$	218.5 V
		$V_{AC,max,PV}$	241.5 V

In the following, four different simulations are proposed.

4.1. Simulation A: Load Increase 1

The first simulation wants to highlight a load increase at time t = 0.5 s. With a load resistance change from 4 to 3 Ω, the increase is such that the variation of the ST power from 12 to 23 kW satisfies the load and the MT and PV maintain the power generated previously, as defined by the described logics. The initial working point is specified by the load flow assignments and reported in Table 9.

Table 9. Power production variation to achieve the objective. Values shown considered rated voltage.

	Initial Value	Final Value
P_{load}	36 kW	45 kW
Load resistance	4 Ω	3 Ω
$P_{MT,DC}$	10 kW	10 kW
$P_{ST,DC}$	12 kW	23 kW
$P_{PV,DC}$	15.8 kW	15.8 kW

From Figures 6–8, it can be easily checked that the load variation is absorbed by the ST and the frequencies are automatically restored to 50 Hz. The AC voltages at steady state are kept inside their limits.

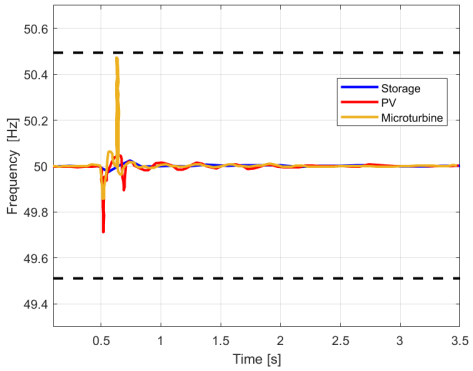

Figure 6. Simulation A: Frequencies. The dashed black lines represent the frequency limits f_{min} and f_{max}.

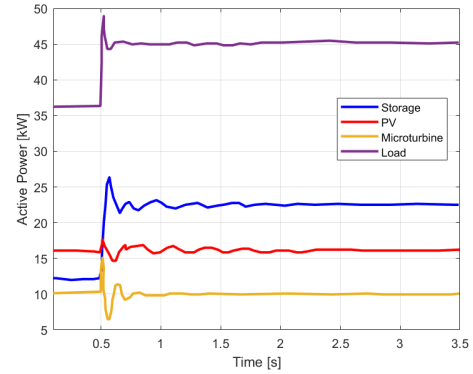

Figure 7. Simulation A: Active Power.

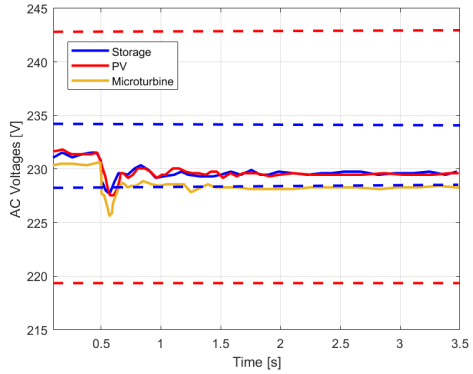

Figure 8. Simulation A: AC Voltages. The blue dashed lines represent $V_{ac,ST,max}$ and $V_{ac,ST,min}$, while the red dashed lines represent $V_{ac,PV,max}$ and $V_{ac,PV,min}$.

4.2. Simulation B: Load Increase 2

The next simulation (Figure 9) shows a load increase at the time t = 0.5 s with a change in the load resistance from 4 to 1.5 Ω. The increase is such that the ST variation is no longer sufficient and the MT must also intervene to satisfy the demand. The ST reaches its maximum (60 kW), and the MT moves its production from 10 to 16 kW, as defined by the previous logic.

The initial working points are specified by the load flow assignments and reported in Table 10.

Table 10. Power production variation to achieve the objective.

	Initial Value	Final Value
P_{load}	36 kW	80 kW
Load resistance	4 Ω	1.5 Ω
$P_{MT,DC}$	10 kW	16 kW
$P_{ST,DC}$	12 kW	60 kW
$P_{PV,DC}$	15.8 kW	15.8 kW

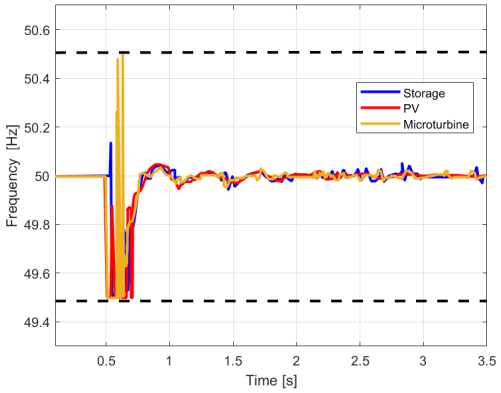

Figure 9. Simulation B: Frequencies. The dashed black lines represent the frequency limits f_{min} and f_{max}.

As shown in Figure 10, the ST reaches its limit in terms of maximum power, and consequently, the MT increases its production. The AC voltages (Figure 11) are kept below their limits at steady state, while a short transient decrease can be observed when the load changes.

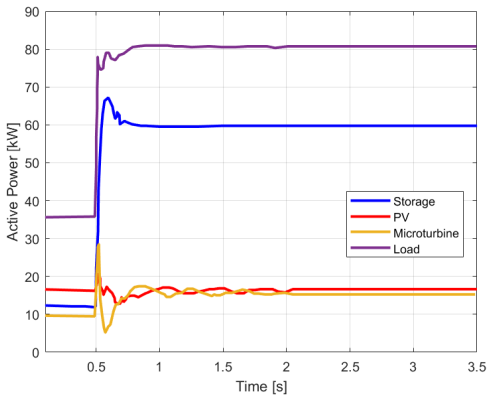

Figure 10. Simulation B: Active Power.

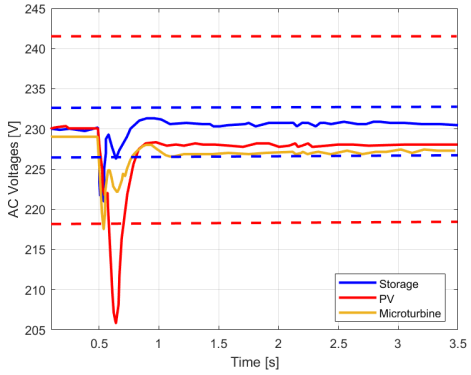

Figure 11. Simulation B: AC Voltages. The blue dashed lines represent $V_{ac,ST,max}$ and $V_{ac,ST,min}$, while the red dashed lines represent $V_{ac,PV,max}$ and $V_{ac,PV,min}$.

4.3. Simulation C: Load Decrease 1

Moving from a load resistance of 4 to 5 Ω (Figures 12–14), the MT decreases the power supplied from 10 to 4.8 kW, while ST and PV remain at their reference values, as defined by the logics. The initial working point is specified by the load flow assignments and reported in Table 11.

Table 11. Power production variation to achieve the objective.

	Initial Value	Final Value
P_{load}	36 kW	19 kW
Load resistance	4 Ω	5 Ω
$P_{MT,DC}$	10 kW	4.8 kW
$P_{ST,DC}$	12 kW	12 kW
$P_{PV,DC}$	15.8 kW	15.8 kW

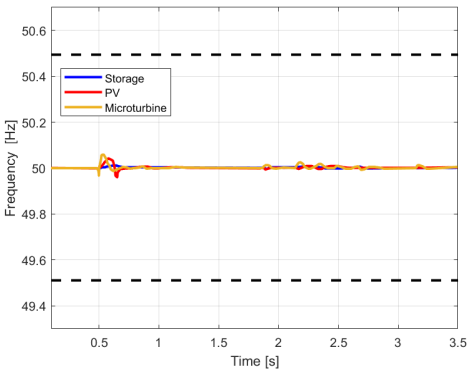

Figure 12. Simulation C: Frequencies. The dashed black lines represent the frequency limits f_{min} and f_{max}.

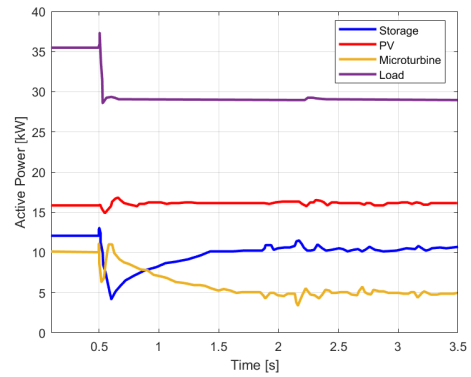

Figure 13. Simulation C: Active Power.

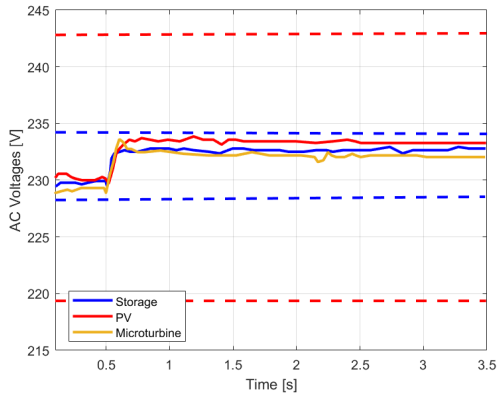

Figure 14. Simulation C: AC Voltages. The blue dashed lines represent $V_{ac,ST,max}$ and $V_{ac,ST,min}$, while the red dashed lines represent $V_{ac,PV,max}$ and $V_{ac,PV,min}$.

4.4. Simulation D: Load Decrease 2

In the case of a greater load reduction, the reduction of the MT power is no longer sufficient, and also, the ST must decrease its power production. Moving from a resistance of 4 to 6 Ω, the MT decreases the power until it goes off (0 kW), the ST changes from 12 to 10 kW, and the PV maintains the power to the MPPT reference. The initial working point is specified by the load flow assignments and reported in Table 12.

Table 12. Power production variation to achieve the objective.

	Initial Value	**Final Value**
P_{load}	36 kW	25 kW
Load resistance	4 Ω	6 Ω
$P_{MT,DC}$	10 kW	0 kW
$P_{ST,DC}$	12 kW	10 kW
$P_{PV,DC}$	15.8 kW	15.8 kW

Figures 15–17 show the turn-off of the MT (its production is 0 kW) and the decrease of the ST unit in order to satify the load balance. Once again, frequencies and AC voltages are kept below their limits.

With respect to the work proposed in [15], where the MT was not included, some further oscillations can be observed especially in simulation B, when the load varies from 36 to 80 kW. On the other hand, the time needed for reaching the steady state in the proposed simulations is comparable with the ones described in [15].

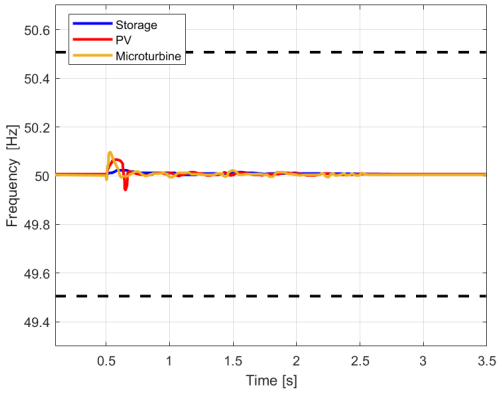

Figure 15. Simulation D: Frequencies. The dashed black lines represent the frequency limits f_{min} and f_{max}.

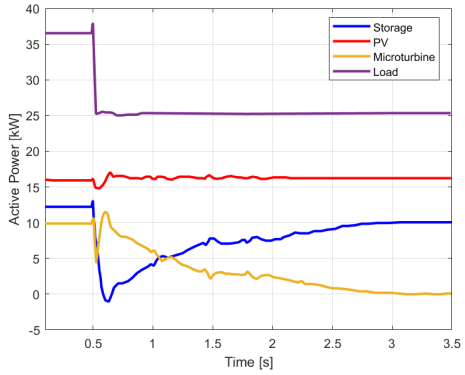

Figure 16. Simulation D: Active Power.

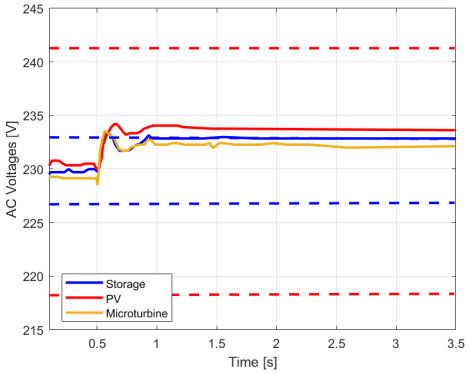

Figure 17. Simulation D: AC Voltages. The blue dashed lines represent $V_{ac,ST,max}$ and $V_{ac,ST,min}$, while the red dashed lines represent $V_{ac,PV,max}$ and $V_{ac,PV,min}$.

5. Conclusions

We proposed an inovvative control system, based on the MPC technique, that is able to control the behavior of an MG made of three different units (PV, ST and MT) without relying on communication between the sources. Having the possibility of restoring voltage and frequency without the need of a communication link among devices and without a slower secondary control level makes the proposed approach appealing for an MG installed in rural areas. The main differences with respect to traditional methods are shown in Table 13. The transition between different modes is achieved by means of automatic switch. We validated the proposed control system by means of a comparison with the Simulink/Simscape environment. Future work will involve the extension of the proposed MPC controllers with different control issues (e.g., Demand/Response strategies) as well as the validation of the proposed approach in experimental testbed facilities and a more complex validation model where the MT is no longer considered as an ideal current generator but as a permanent magnet generator with two inverters.

Table 13. Pros and cons of the control methods: DC: Droop Control, MSC: Master–Slave Control.

	+	−
DC	No communication Low model dependence	Steady-state errors
MSC	No steady-state errors	Need of communication
MPC	No communication No steady-state errors	Average model dependence

Author Contributions: Conceptualization, D.M., R.P. and A.R.; methodology, D.M. and R.P.; software, I.X. and D.M.; validation, I.X.; formal analysis, A.B.; investigation, A.B.; data curation, I.X.; writing—original draft preparation, D.M.; writing—review and editing, R.P.; supervision, R.P.; funding acquisition, A.B. All authors have read and agreed to the published version of the manuscript.

Funding: This research received no external funding.

Institutional Review Board Statement: Not applicable.

Informed Consent Statement: Not applicable.

Data Availability Statement: Not applicable.

Conflicts of Interest: The authors declare no conflict of interest.

References

1. Thema, J.; Suerkemper, F.; Couder, J.; Mzavanadze, N.; Chatterjee, S.; Teubler, J.; Thomas, S.; Ürge-Vorsatz, D.; Hansen, M.B.; Bouzarovski, S.; et al. The multiple benefits of the 2030 EU energy efficiency potential. *Energies* **2019**, *12*, 2798. [CrossRef]
2. Bueno, P.G.; Hernández, J.C.; Ruiz-Rodriguez, F.J. Stability assessment for transmission systems with large utility-scale photovoltaic units. *IET Renew. Power Gener.* **2016**, *10*, 584–597. [CrossRef]
3. Hernández, J.C.; Sanchez-Sutil, F.; Vidal, P.; Rus-Casas, C. Primary frequency control and dynamic grid support for vehicle-to-grid in transmission systems. *Int. J. Electr. Power Energy Syst.* **2018**, *100*, 152–166. [CrossRef]
4. Adam, K.; Müller-Mienack, M.; Paun, M.; Sanchis, G.; Strunz, K. e-HIGHWAY 2050—The ENTSO-E facilitated study programme towards a Modular Development Plan on pan-European Electricity Highways System 2050. In Proceedings of the 2012 IEEE Power and Energy Society General Meeting, San Diego, CA, USA, 22–26 July 2012; IEEE: Piscataway, NJ, USA, 2012; pp. 1–6.
5. Jiayi, H.; Chuanwen, J.; Rong, X. A review on distributed energy resources and MicroGrid. *Renew. Sustain. Energy Rev.* **2008**, *12*, 2472–2483. [CrossRef]
6. Vandoorn, T.; De Kooning, J.; Meersman, B.; Vandevelde, L. Review of primary control strategies for islanded microgrids with power-electronic interfaces. *Renew. Sustain. Energy Rev.* **2013**, *19*, 613–628. [CrossRef]
7. Mortezaei, A.; Simões, M.G.; Savaghebi, M.; Guerrero, J.M.; Al-Durra, A. Cooperative control of multi-master–slave islanded microgrid with power quality enhancement based on conservative power theory. *IEEE Trans. Smart Grid* **2016**, *9*, 2964–2975. [CrossRef]
8. Peyghami, S.; Mokhtari, H.; Loh, P.C.; Davari, P.; Blaabjerg, F. Distributed primary and secondary power sharing in a droop-controlled LVDC microgrid with merged AC and DC characteristics. *IEEE Trans. Smart Grid* **2016**, *9*, 2284–2294. [CrossRef]
9. Rocabert, J.; Luna, A.; Blaabjerg, F.; Rodriguez, P. Control of power converters in AC microgrids. *IEEE Trans. Power Electron.* **2012**, *27*, 4734–4749. [CrossRef]
10. Hatziargyriou, N. *Microgrids: Architectures and Control*; John Wiley & Sons: Hoboken, NJ, USA, 2014.
11. Camacho, E.F.; Alba, C.B. *Model Predictive Control*; Springer: Berlin/Heidelberg, Germany, 2013.
12. Zhang, Y.; Meng, F.; Wang, R.; Kazemtabrizi, B.; Shi, J. Uncertainty-resistant stochastic MPC approach for optimal operation of CHP microgrid. *Energy* **2019**, *179*, 1265–1278. [CrossRef]
13. Babqi, A.J.; Etemadi, A.H. MPC-based microgrid control with supplementary fault current limitation and smooth transition mechanisms. *IET Gener. Transm. Distrib.* **2017**, *11*, 2164–2172. [CrossRef]
14. Nguyen, T.T.; Yoo, H.J.; Kim, H.M. Application of model predictive control to BESS for microgrid control. *Energies* **2015**, *8*, 8798–8813. [CrossRef]
15. Rosini, A.; Mestriner, D.; Labella, A.; Bonfiglio, A.; Procopio, R. A decentralized approach for frequency and voltage regulation in islanded PV-Storage microgrids. *Electr. Power Syst. Res.* **2021**, *193*, 106974. [CrossRef]
16. Shan, Y.; Hu, J.; Li, Z.; Guerrero, J.M. A model predictive control for renewable energy based AC microgrids without any PID regulators. *IEEE Trans. Power Electron.* **2018**, *33*, 9122–9126. [CrossRef]
17. Heydari, R.; Khayat, Y.; Naderi, M.; Anvari-Moghaddam, A.; Dragicevic, T.; Blaabjerg, F. A decentralized adaptive control method for frequency regulation and power sharing in autonomous microgrids. In Proceedings of the 2019 IEEE 28th International Symposium on Industrial Electronics (ISIE), Vancouver, BC, Canada, 12–14 June 2019; IEEE: Piscataway, NJ, USA, 2019; pp. 2427–2432.
18. Bonfiglio, A.; Delfino, F.; Labella, A.; Mestriner, D.; Pampararo, F.; Procopio, R.; Guerrero, J.M. Modeling and Experimental Validation of an Islanded No-Inertia Microgrid Site. *IEEE Trans. Sustain. Energy* **2018**, *9*, 1812–1821. [CrossRef]
19. Guo, X.; Guo, H. Simulation and control strategy of a micro-turbine generation system for grid connected and islanding operations. *Energy Procedia* **2011**, *12*, 368–376. [CrossRef]
20. Bonfiglio, A.; Brignone, M.; Invernizzi, M.; Labella, A.; Mestriner, D.; Procopio, R. A simplified microgrid model for the validation of islanded control logics. *Energies* **2017**, *10*, 1141. [CrossRef]